

Blade Shape Optimization for HSI Noise Reduction and Performance Improvement of Helicopter

Sanghyun Chae(nyugnas@korea.com) and Kwanjung Yee(daedalus@pusan.ac.kr)
Department of Aerospace Engineering, Pusan National University
Pusan, Korea

Choongmo Yang(yang@chofu.jaxa.jp) and Takashi Aoyama(aoyama@chofu.jaxa.jp)
Numerical Analysis Group, Japan Aerospace Exploration Agency (JAXA)
Tokyo, Japan

Shinkyu Jeong(jeong@edge.ifs.tohoku.ac.jp) and Shigeru Obayashi(obayashi@ieee.org)
Institute of Fluid Science, Tohoku University
Miyagi, JAPAN

Abstract

A high speed impulsive (HSI) noise occupies much part of the loudest noise of helicopter. It is caused by the shock wave on a blade surface at the advancing side and limits high speed flight performance of helicopter. To reduce the HSI noise, the authors performed blade planform design by using an aero-acoustic analysis technique and an optimization method. As for the aero-acoustic analysis, CFD technique for aerodynamic analysis and Kirchhoff's method for the acoustic analysis were used. As for the optimization method, Kriging-based genetic algorithm (GA) model as a high-fidelity multi-objective optimization method was chosen according to the design problem. In the present research, design variables to define arbitrary blade planform and new design variable to describe airfoil transition were used to consider the aerodynamic performance and noise characteristic, simultaneously. The optimization results showed that optimum blades have improved aerodynamic performance and similar level of HSI noise characteristic compared to the optimum shape obtained in our previous research.

Nomenclature

A : area of rotor disk
c : chord length of airfoil
 $d(\mathbf{x}^i, \mathbf{x}^j)$: weighted distance between vector \mathbf{x}^i and \mathbf{x}^j
 l_n : likelihood function of Kriging model
 M_T : torsional moment of rotorcraft
 N_B : number of blade
T : thrust of rotorcraft
R : radius of rotor
 $s^2(\mathbf{x})$: mean squared error in Kriging model
 \mathbf{x} : m -dimensional vector of design variables
 $y(\mathbf{x})$: unknown function of Kriging model
 $\hat{y}(\mathbf{x})$: estimated value of $y(\mathbf{x})$
 $Z(\mathbf{x})$: a local deviation from the global model in Kriging model
 Ω : rotating speed of rotor
 Φ : standard normal distribution function
 β : a constant of global model in Kriging model
 $\hat{\beta}$: estimated value of β
 ρ : air density
 σ : solidity of rotor, $\sigma = \frac{N_B c R}{\pi R^2}$
 $\hat{\sigma}^2$: variance of Kriging model
 $\boldsymbol{\theta}$: correlation parameter vector

ϕ : density function of the normal distribution, the Gaussian function

Introduction

Helicopter is a utility air vehicle, which has more efficient hovering and vertical flight abilities than other types of air vehicle. These outstanding features make helicopter to conduct some special missions such as fire fighting, rescue, broadcasting etc., as well as transportation and commuter. However, noise of helicopter is one of the obstructions which decrease the range of helicopter application. The high speed impulsive (HSI) noise is the most serious noise sources of a helicopter rotor. This loud noise limits forward flight speed and downtown accessibility of helicopter. The HSI noise problem is caused by the propagation of shock wave on an advancing blade surface to farfield as shown in Fig.1. Figure 2 shows wave form of the HSI noise at different Mach number of blade tip. The distribution of acoustic pressure has a negative peak and the absolute value of this minimum peak is increased by strong shock wave. Thus this minimum peak value indicates the quantity of noise. The details of HSI noise were summarized by Schmitz and Yu^[1]. They reviewed the status of HSI noise studies in 1980s, when researches on the HSI noise were massively conducted by theoretical and experimental approaches.

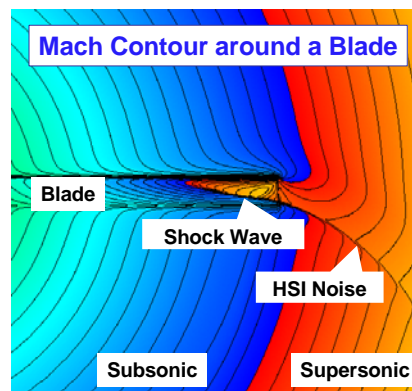


Fig.1: HSI noise generation

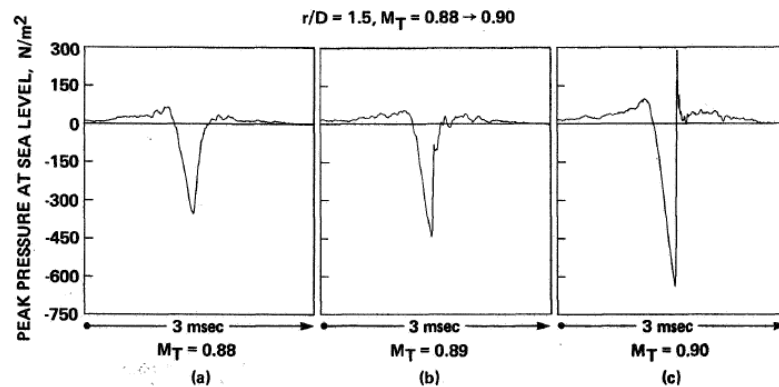


Fig.2: Waveform of HSI noise^[1]

Former research works^[1-3] showed that modification of blade planform near tip can reduce the intensity of the HSI noise. These parametric studies were conducted by using simple variables, such as swept back angle, and taper ratio. Following researches^[4-6] have adapted optimization methods, which have been used in aerodynamics and structure to search an optimum shape for noise reduction. As a research to achieve better blade design for noise reduction or performance improvement or both, optimization techniques with aerodynamic and/or acoustic analysis tool have been developed up to now. Lee and Kwon^[4] used optimization technique to obtain a rotor blade configuration which minimized the required inviscid torque under the constraint of maintaining the desired thrust level, but they focused only on the improvement of performance. Xue et al.^[5] developed an integrated aero-acoustics rotor simulation tool by combining COPTER code for rotorcraft performance and a full potential rotor code for unsteady 3D transonic flows around rotor blade, but the shock wave captured by potential code was not strong enough to represent HSI noise. Collins et al.^[6] showed Pareto frontier method by using both low and high fidelity analysis tools to examine a redesign of the HART model rotor. However, this research showed only the redesign of a rotor similar to the BO-105 using simple

shape design variables. Therefore, the need of more accurate design tool is increasing for a general blade shape design with multi-objective optimization in order to consider both noise and performance simultaneously.

In our previous research^[7], an arbitrary planform design was conducted to reduce HSI noise, but aerodynamic performance was not considered. In the present paper, we construct a design tool for arbitrary blade shapes using CFD technique and multi-objective optimization considering both performance and noise simultaneously. Based on our previous research, an optimum 3D blade shape with modification of blade planform and variation of airfoil section is obtained by using CFD technique for aerodynamic analysis, Kirchhoff's method for acoustic analysis, and Kriging-based genetic algorithm (GA) for optimization method.

Numerical Analysis

Aerodynamics

For the prediction of near field pressure around blade, CFD calculation on the accurate flowfield around a blade was conducted. The governing equation in the CFD solver was three dimensional unsteady Euler equations in rotating curvilinear coordinates fixed on a blade. A diagram of Cartesian coordinate system (x, y, z) and curvilinear coordinate system (ξ, η, ζ) of rotating blade are shown in Fig. 3. The numerical method to solve the governing equation was an implicit finite difference scheme. A higher-order upwind TVD scheme was applied for the inviscid terms of the explicit right-hand side. The accuracy of this solver was second order in space and first order in time. To obtain an unsteady solution in forward flight, Newton iterative method with four iterations was used at each time step to improve the accuracy in time. The details of CFD solver were reviewed in a previous paper^[8].

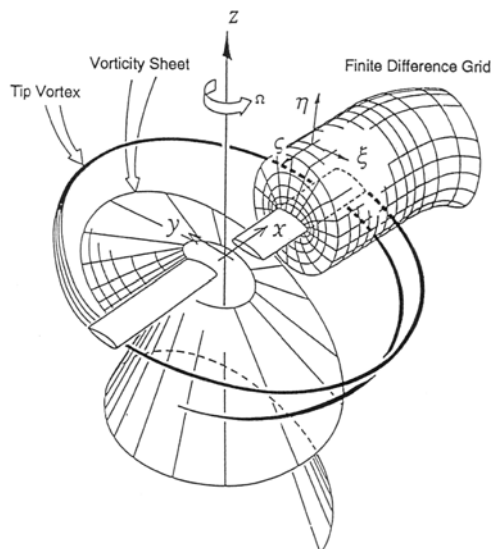


Fig.3: Blade coordinate system and grid

Figure 4 shows the perspective and top views of O-H type grid used for the CFD calculation and blade tip grid of modified shape. The baseline blade as a reference had a rectangular planform based on UH-1H which is simple and widely used. The airfoil section of baseline blade was fixed to NACA0012 with different chord length according to the blade planform in order to eliminate the effect of difference in airfoil section.

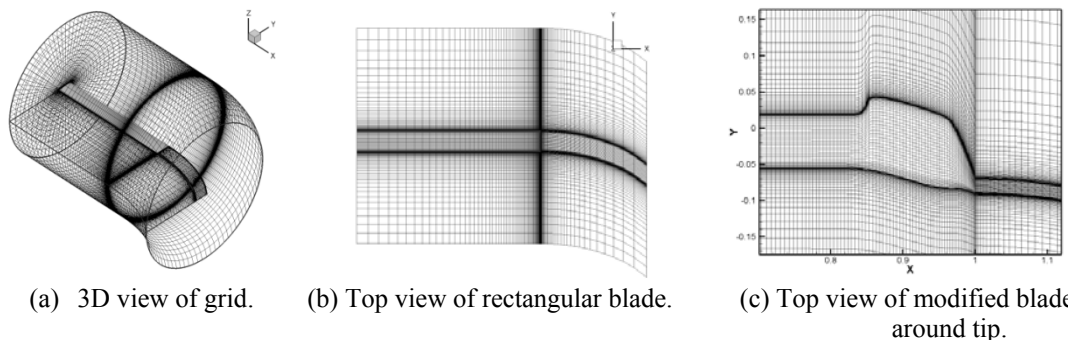


Fig.4: Grid system.

The grid consists of $79 \times 50 \times 140$ points, and 79×100 points were distributed on the blade surface. The aspect ratio of the blade was 13.7. The grid outboard blade tip was swept-back to follow shock wave which is generated on the blade surface and is propagated far away as a HSI noise. This swept-back grid type can impose the high grid density on the disturbance region. The tip Mach number is 0.9.

Acoustics

The near field acoustic prediction was based on the pressure results from CFD calculation. For the far field acoustic prediction, a combining method of CFD with Kirchhoff's equation^[11-13] was used. In this method, a CFD technique was used to obtain the pressure distribution around a rotor blade, then, the Kirchhoff's equation extended for a moving surface was used to find the acoustic pressure at a far-field observer position. The Euler solutions on the Kirchhoff surface, in which all the acoustic sources are enclosed, were used as source pressure data. If the CFD solutions capture the nonlinear effect such as shock wave, this method can predict the acoustic pressure including the effect of these nonlinear sources. Figure 5 shows the Kirchhoff surface which is supposed to include flowfield with noise sources.

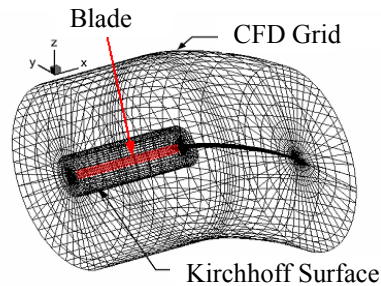


Fig.5: Kirchhoff surface in grid system.

Optimization Technique

Optimization procedure

To solve the constrained multi-objective optimization problem efficiently, we choose a Kriging based genetic algorithm method^[14].

The Kriging model, one of approximation models, predicts the distribution function at an unknown point instead of the function values itself. Using approximation models is known to attract a large attention in the field of aircraft design because it saves a quite amount of computational time for evaluation of objective function. However, it is apt to miss the true optimum in the design space if the exploration relies only on the estimated function values of the approximation model, because these values include uncertainty at unknown point. To overcome this demerit, the criterion of 'expected improvement (EI)' was used with GA exploration. EI expects the function value and its uncertainty at unknown points from the distribution of function values. By selecting maximum EI point as an additional sample point of the Kriging model, the improvement of accuracy and the robust exploration of the true optimum can be achieved at the same time.

Overall procedure of the optimization is the following as shown in Fig. 6.

1. Initial sample points are selected by 'Improved Distributed Sampling'^[15].
2. Sample points are evaluated by CFD solver.
3. Kriging Model is constructed with sample points.
4. GA starts: Initial population is generated and evaluated on Kriging model.
5. Parents are selected.
6. Crossover and mutation.
7. Evaluate the fitness of new generation.
8. If number of generation is not over 100, repeat procedure from 4.
9. Additional sample points are selected using EI by user.
10. Repeat procedure from 2 until the optimums of Kriging model are not updated for 5 iterations. The validity of Kriging model is evaluated by cross-validation.

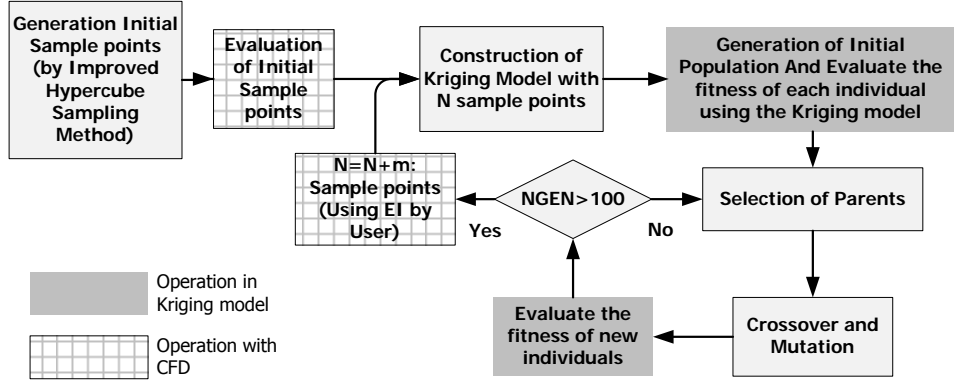


Fig.6: Optimization procedure.

Genetic Algorithm (GA)

Genetic algorithm (GA)^[16] is a searching mechanism based on natural selection and genetics. GA uses the objective function value itself, not its derivative information. This feature makes GA robust and attractive to the aerodynamic design problems where non-linearity, multi-modality, and discontinuities may exist. Another merit of GA is that it searches the optimum point from a population of points, not a single point. It makes GA a promising method for multi-objective (MO) problems. The population of points can represent Pareto optimal set of MO problems^[17]. The definition of Pareto optimality is as follow:

Suppose $\mathbf{x}^1 = (x_1^1, x_2^1)$ and $\mathbf{x}^2 = (x_1^2, x_2^2)$ are in the population and $F = (f_1, f_2)$ is a set of objective functions to be maximized.

1. \mathbf{x}^1 is said to be ‘dominated’ by \mathbf{x}^2 , if $F(\mathbf{x}^1)$ is partially less than $F(\mathbf{x}^2)$, i.e., $f_1(\mathbf{x}^1) \leq f_1(\mathbf{x}^2) \cap f_2(\mathbf{x}^1) \leq f_2(\mathbf{x}^2)$ and $F(\mathbf{x}^1) \neq F(\mathbf{x}^2)$.
2. \mathbf{x}^1 is said to be ‘non-dominated’ if there doesn’t exist \mathbf{x}^2 in the population that dominates \mathbf{x}^2 .

Each point in the Pareto set is optimal in the sense that no improvement can be achieved in any objective function without degradation in the others.

The general procedure of the genetic algorithms is shown in Fig. 7.

1. Creation of initial population
2. Evaluation of fitness (objective) function
3. Selection of parents according to the rank (fitness)
4. Crossover and mutation
5. Check the convergence. If not converged, return to the process No. 2.

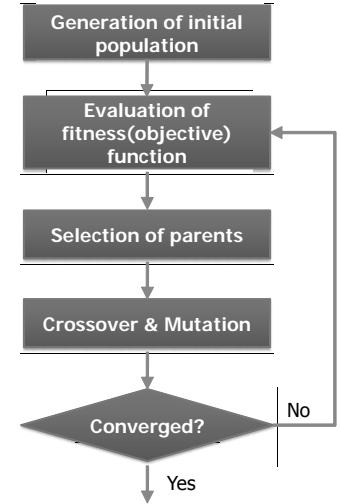


Fig.7: Flow chart of Genetic Algorithm.

Once the optimization is over, the validity of the search region is examined using Kriging model.

Kriging Model

The Kriging model expresses the unknown function $y(\mathbf{x})$ as

$$y(\mathbf{x}) = \beta + Z(\mathbf{x}) \quad (4)$$

where, \mathbf{x} is an m -dimensional vector (m design variables), β is a constant global model, and $Z(\mathbf{x})$ represents a local deviation from the global model. In the model, the local deviation at an unknown point, \mathbf{x} , is expressed using stochastic processes. The sample points are interpolated with the Gaussian random function as the correlation function to estimate the trend of the stochastic processes. The correlation between $Z(\mathbf{x}^i)$ and $Z(\mathbf{x}^j)$ is strongly related to the distance between the two corresponding points, \mathbf{x}^i and \mathbf{x}^j . In the Kriging model, a special weighted distance is used instead of the Euclidean distance, as follows:

$$d(\mathbf{x}^i, \mathbf{x}^j) = \sum_{k=1}^m \theta_k |x_k^i - x_k^j|^2 \quad (5)$$

where, θ_k ($0 \leq \theta_k \leq \infty$) is the k th element of the correlation vector parameter $\boldsymbol{\theta}$. By using the specially weighted distance and the Gaussian random function, the correlation between the point \mathbf{x}^i and \mathbf{x}^j is defined as

$$\text{Corr} [Z(\mathbf{x}^i), Z(\mathbf{x}^j)] = \exp [-d(\mathbf{x}^i, \mathbf{x}^j)]. \quad (6)$$

Kriging predictor^[18], in other word a function estimated by Kriging model, can be expressed as

$$\hat{y}(\mathbf{x}) = \hat{\beta} + \mathbf{r}'\mathbf{R}^{-1}(\mathbf{y} - \mathbf{1}\hat{\beta}) \quad (7)$$

where, $\hat{\beta}$ is the estimated value of β , \mathbf{R} denotes the $n \times n$ matrix whose (i,j) entry is $\text{Corr}[Z(\mathbf{x}^i), Z(\mathbf{x}^j)]$. The i -th element of vector \mathbf{r} is

$$r_i(\mathbf{x}) \equiv \text{Corr}[Z(\mathbf{x}), Z(\mathbf{x}^i)] \quad (8)$$

and $\mathbf{y} = [y(x^1), \dots, y(x^n)]$.

Detailed derivation of the above equations is in Ref.19. The unknown parameter to be estimated for constructing the Kriging model is $\boldsymbol{\theta}$. This parameter can be estimated by maximizing the following likelihood function

$$\text{Ln}(\hat{\beta}, \hat{\sigma}^2, \boldsymbol{\theta}) = -\frac{n}{2} \ln(2\pi) - \frac{1}{2} \ln(|\mathbf{R}|) - \frac{n}{2} \ln(\hat{\sigma}^2) - \frac{1}{2\hat{\sigma}^2} (\mathbf{y} - \mathbf{1}\hat{\beta})' \mathbf{R}^{-1} (\mathbf{y} - \mathbf{1}\hat{\beta}) \quad (9)$$

where, $\mathbf{1}$ denotes an m -dimensional unit vector.

Maximizing the likelihood function is an m -dimensional unconstrained non-linear optimization problem. In this paper, GA is adapted to solve the present problem. The accuracy of the prediction value largely depends on the distance from the sample points. Intuitively speaking, the closer the point \mathbf{x} is to the sample points, the more accurate the prediction $\hat{y}(\mathbf{x})$ is. This intuition is expressed in following equation,

$$s^2(\mathbf{x}) = \hat{\sigma}^2 \left[1 - \mathbf{r}'\mathbf{R}^{-1}\mathbf{r} + \frac{(1 - \mathbf{1}'\mathbf{R}^{-1}\mathbf{r})^2}{\mathbf{1}'\mathbf{R}^{-1}\mathbf{1}} \right] \quad (10)$$

where, $s^2(\mathbf{x})$ is the mean squared error of the predictor. It indicates the uncertainty at the estimation point. The root mean squared error (RMSE) is expressed as $s = \sqrt{s^2(\mathbf{x})}$.

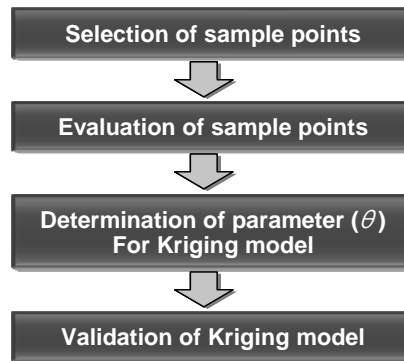


Fig.8: Procedure to improve Kriging model

Figure 8 shows the procedure to improve Kriging model using the sample points which are added after GA. First, a sample population is generated by improved hypercube sampling. This method selects sample points to be scattered inside the interval partitioned on search space. The distribution of design variables is investigated and the validity of the search region is checked. If the search region is invalid, it is redefined. Second step is the evaluations of the objective functions at the sample points using CFD solver and Kirchhoff method. With the sample data obtained from the analysis modules, the Kriging parameter, θ , is determined by solving

maximization problem of Eq.(9). Once the model is constructed, the model should be validated. The validation is performed by the cross validation^[19]. If the model is valid, all cross-validated values should lie inside of the confidence region. It can be check by using the “standardized cross-validated residual” as follows.

$$\frac{y(x_i) - \hat{y}_{-i}(x_i)}{S_{-i}(x_i)} \quad (11)$$

If residual is not in the confidence range, a few additional sample points should be selected from the extended region of the redefined search region to ensure the accuracy of the Kriging models. This routine is iterated until Kriging model is valid.

Exploration of the global optimization and improvement of the model

Once the approximation model is constructed, the optimum point can be explored using an arbitrary optimizer on the model. However, it is possible to miss the global optimum because the approximation model includes uncertainty at the predicted point.

In Fig. 9, the real shape of objective function and predicted shape by the Kriging model are compared. Eight points are selected for constructing the Kriging model. The minimum point on the Kriging model is located near $x=9$, whereas the real global minimum of the objective function is sited near $x=4$. However it is hard to search the global minimum on the present Kriging model, the real global minimum near $x=4$ cannot be found. For a robust search of the global optimum, the predicted value by the Kriging model and its uncertainty should be considered at the same time.

Figure 10 shows the predicted value and the standard error of the Kriging model. Around $x=9.5$, the standard error of the Kriging model is very small because there are many sample points around this point. Thus, the confidence interval is very short as shown in Figure 10. On the other hand, the standard error is very large around $x=3.5$ due to the lack of sample points around there. Thus, the confidence interval at this point is very wide. The minimum inside this interval is less than the present minimum point on the Kriging model. This point has somewhat a large probability to become the global minimum.

This concept is expressed in the criterion of EI^[20]. The EI of minimization problem can be calculated as follows:

$$E[I] = (f_{\min} - \hat{y}) \Phi\left(\frac{f_{\min} - \hat{y}}{s}\right) + s \phi\left(\frac{f_{\min} - \hat{y}}{s}\right), \quad (11)$$

where, f_{\min} is the minimum value among n sampled values. The values of Φ and ϕ are the standard distribution and normal density, respectively. By selecting the maximum EI value point as an additional sample point, the robust exploration of the global optimum and the improvement of model can be achieved simultaneously.

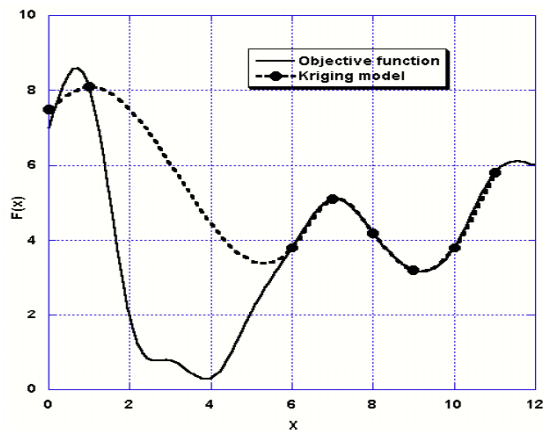


Fig.9: Objective function and Kriging model

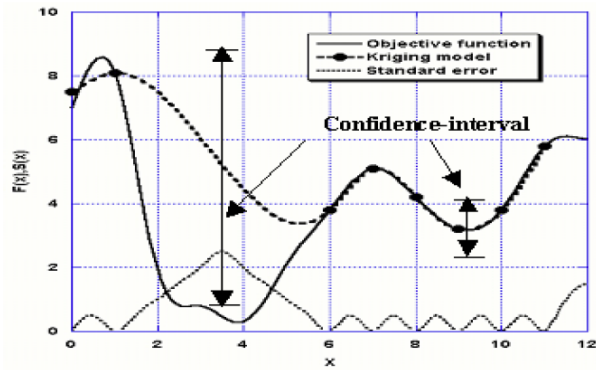


Fig.10: Predicted value and standard error of Kriging model

Definition of Design Problem

Objective functions

The optimization in the present paper aimed to improve HSI noise characteristics and aerodynamic performance simultaneously. For a practical evaluation for noise characteristics and aerodynamic performance, two objective functions were selected.

One of objective functions was the absolute value of minimum acoustic pressure and it should be minimized to reduce HSI noise. For the efficient evaluation of HSI noise, two assumptions were used. The characteristics of HSI noise was evaluated using non-lifting blade in hovering condition. Because the former research works^[1-3] showed that the HSI noise can be simply simulated by using non-lifting blade in hovering condition. This fact removed the burden of trim analysis in forward flight. And the noise characteristics were calculated by the CFD solver at $r=1.11R$ as an evaluation point. Practical evaluation of the far-field HSI noise should be executed by noise analysis technique such as Kirchhoff method, but an alternative way to speed up the optimization process was to use an acoustic pressure calculated by the CFD solver at the proper observer position, which can evaluate the far-field HSI noise^[7].

The other objective function for the evaluation of aerodynamic characteristics was thrust coefficient per solidity of modified blade. The aerodynamic evaluation was conducted at a fixed non-zero angle of attack (2° in the present calculations) to avoid large calculation for trim analysis. This coefficient was defined as follows.

$$C_T / \sigma = \frac{T}{\rho A \Omega^2 R^2} \left/ \left(\frac{N_B c R}{\pi R^2} \right) \right. \quad (12)$$

Design Variables

Three dimensional blade shape was considered by 14 design variables to describe arbitrary planform shape and airfoil transition from NACA0012 to NACA0008, as shown in Fig. 11. The 14 design variables were used to describe an arbitrary planform shape using cubic B-spline from 0.5R. Transition range between the two airfoils was 0.06R, and its center was defined as the 15th design variable. Combination of airfoil section was introduced to consider the different aerodynamic characteristics along the blade span due to blade rotation. In the present work, effect of airfoil thickness was only considered. The upper bound and lower bound of each design variables was defined as shown in table 2.

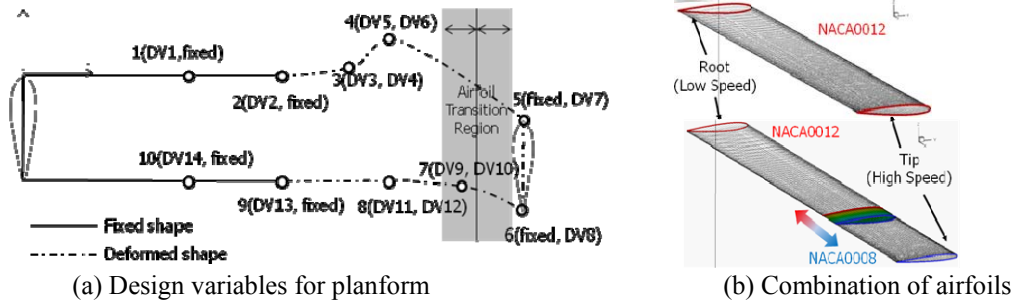


Fig.11: Definition of design variables

Table 2: Upper and lower bound of design variables

Variables	Description	Constraint	Variables	Description	Constraint
DV1	X position of point 1	$0.0R \leq DV1 \leq 0.5R$	DV9	X position of point 7	$DV11 \leq DV9 \leq 0.97$
DV2	X position of point 2	$0.5R \leq DV2 \leq DV3$	DV10	Y position of point 7	$-1.4C \leq DV6 \leq 0.7C$
DV3	X position of point 3	$DV2 \leq DV3 \leq DV5$	DV11	X position of point 8	$DV13 \leq DV11 \leq 0.98$
DV4	Y position of point 3	$-0.3C \leq DV4 \leq 0.4C$	DV12	Y position of point 8	$-1.4C \leq DV12 \leq 0.7C$
DV5	X position of point 4	$DV3 \leq DV5 \leq 0.97$	DV13	X position of point 9	$0.5R \leq DV13 \leq DV11$
DV6	Y position of point 4	$-0.3C \leq DV6 \leq 0.4C$	DV14	X position of point 10	$0.0R \leq DV14 \leq 0.5R$
DV7	Y position of point 5	$-1.5C \leq DV7 \leq DV9 \leq 0.5C$	DV15	Airfoil Transition	$0.5R \leq DV15 \leq 0.95R$
DV8	Y position of point 6	$-1.5C \leq DV7 \leq DV8 \leq 0.5C$			

Constraints

Four constraints were applied to make reasonable blade planform shape. Three of them were the geometric constraints to define the relations between neighboring points, blade planform area change limit, and curvature limit as a viewpoint of manufacture. The other was a torsional moment coefficient to consider an aerodynamic performance, which is defined as

$$C_{M_T} = \frac{M_T}{\rho A \Omega^2 R^3}, \quad (12)$$

where, M_T means torsional moment. The details of constraints are reviewed in the previous paper^[7].

Results and Discussion

After 12 iterations of optimization procedure, we can obtain 74 sample points. The validity of Kriging model made by the last sample points was evaluated by the cross-validation. Figures 12 (a) and (c) show objective values calculated by the CFD solver on x axis and by the Kriging model on y axis. If points are located near the proportional line of x, y axis, the Kriging model is considered accurate. In Fig. 12 (a), low values of minimum acoustic pressure have larger difference between CFD solver and Kriging model than those of high values. But, it doesn't effect on the optimum solution because the optimum point is the highest value of minimum acoustic pressure. On the other hand, most values of C_T/σ are on the proportional line in Fig. 12 (c). Figures 12 (b) and (d) show standardized cross-validated residual of each objective function on Kriging model. All the residual points for both objective functions on the Kriging model lie in the interval of $[-5, 5]$, which means the prediction of 99.5% confidence.

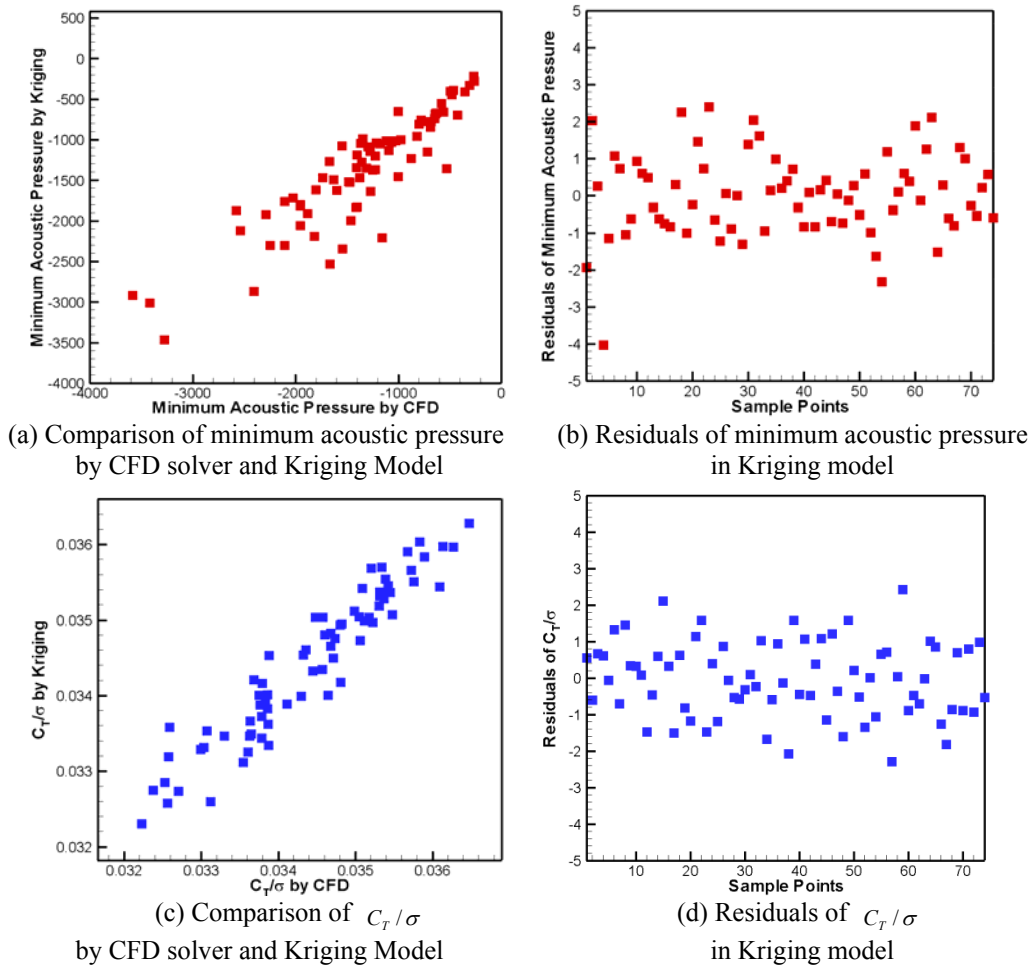


Fig.12: Results of cross-validation

Figure 13 shows minimum acoustic pressure and C_T/σ of all populations including optimum shapes and some special type shapes, such as rectangular, crank, BERP, ONERA, ERATO, and NAL type. The diagonal yellow arrow means the direction of optimization. This diagonal direction expresses optimization conduction for two objective functions simultaneously. In the result, three optimum shapes are selected on the boundary of the last samples. These three shapes have similar values of objective functions as shown in table 3. We name noise optimum shape, C_T/σ optimum shape, and balanced optimum shape of noise and C_T/σ for each performance. Except for C_T/σ optimum, the present optimum shapes had more improved values of objectives than those of our previous optimum^[7] as shown in table 3. Only the case of C_T/σ optimum has more improved aerodynamic performance.

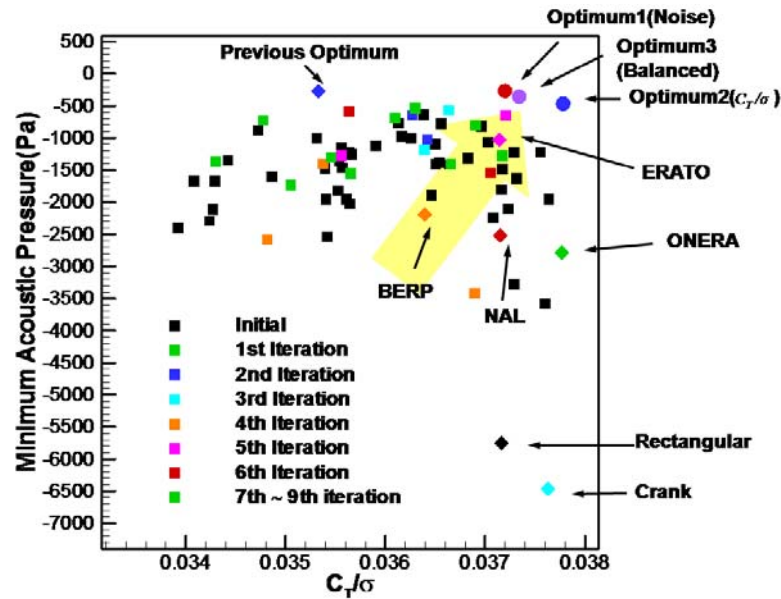


Fig.13: Pareto surface of all population

Table 3: Objective function values of each blade shape

Shape	C_t/σ	Peak Pressure(Pa)	Area
Baseline	0.0372	604	0.07965
Previous Optimum	0.0353(-5%)	-122(-80%)	0.07806(-2%)
Optimum1 (Noise)	0.0372(\pm 0%)	-85(-86%)	0.07777(-2.4%)
Optimum2 (C_T/σ)	0.0384(+3%)	-137(-77%)	0.08068(1.3%)
Optimum3 (Balanced)	0.0380(+2%)	-101(-83%)	0.07686(-3.5%)

※ % in parenthesis means difference form value of baseline

Figure 14 shows acoustic pressure calculated by Kirchhoff's method. The absolute value of minimum acoustic pressure of the optimum shapes shows more than 77% reduction than that of baseline. Figure 15 shows Mach contour comparison among baseline and three optimum shapes. The shock region near blade tip in the Mach contour of rectangular blade is stronger than that of optimums. From these facts, we can confirm that weaker shock wave on optimum blade surface reduces the peak acoustic pressure, and HSI noise of optimum shapes is reduced.

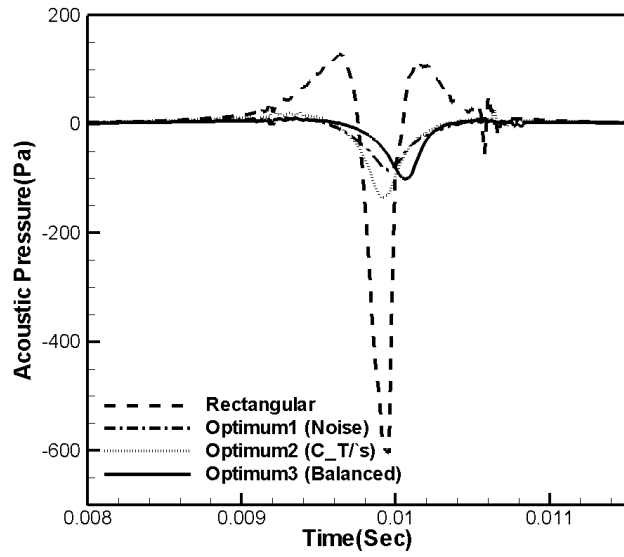


Fig.14: Comparison of acoustic pressure

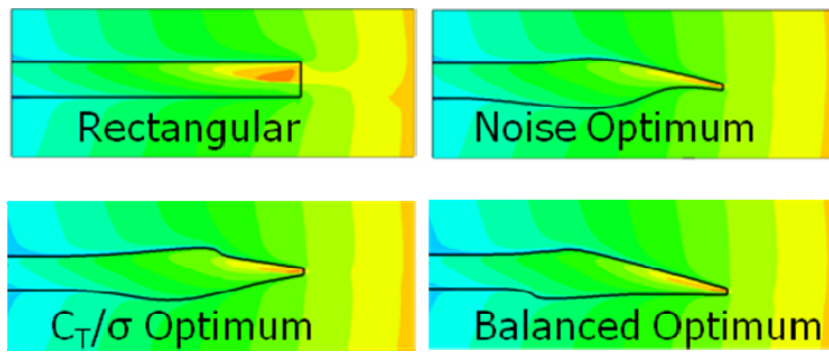


Fig.15: Comparison of Mach contour

Figure 16 shows planform shapes of baseline blade, the previous optimum blade and the present noise optimum blade for comparison of noise optimization results. The swept angle of present optimum shape was significantly reduced than that of previous optimum shape. An airfoil transition region of present shape was from 0.82R to 0.88R. These shape change was caused by airfoil transition. Thick airfoil (NACA0012) has larger lift than thin airfoil (NACA0008), but thin airfoil makes weaker shock wave. Figure 17 shows the relation of trade-off between C_T/σ and HSI noise characteristics by airfoil transition. Thus, the present noise optimum didn't need high sweptback angle by thin airfoil over 0.88R, and simultaneously has more lift by thick airfoil from root until 0.82R. From these results, improvements of both HSI noise characteristic and aerodynamic performance can be obtained by sectional transition of two airfoils.

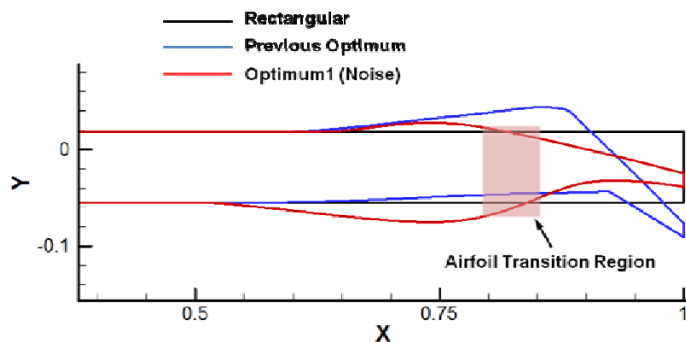


Fig.16: Planform comparison

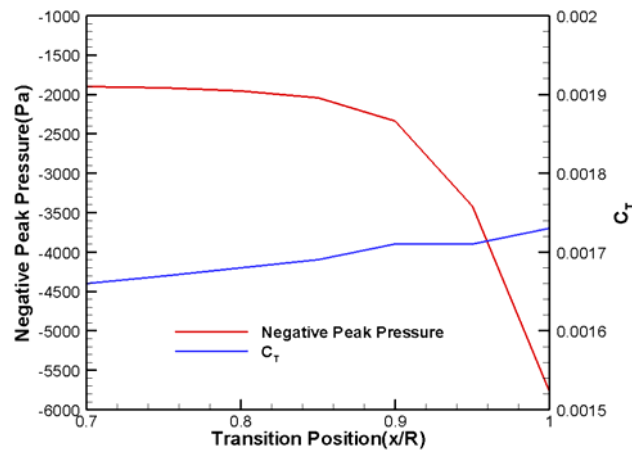


Fig.17: Objective value line changed by airfoil transition position

Summary and Future Works

Based on our previous research, blade planform shape and airfoil transition position was optimized to reduce HSI noise and to improve aerodynamic performance using GA based on Kriging method and CFD technique. As a result of optimization, three optimum blade shapes showed improved value of C_T/σ and HSI noise characteristics, simultaneously. These improvements are caused by airfoil transition between two airfoils with different thickness. Thus, we can see possibility of performance improvement by combination of airfoils without sacrificing HSI noise characteristic using high sweptback angle and high taper ratio.

As a next step, we are extending blade shape optimization with additional design variables such as camber, thickness of two airfoils by using equations of NACA 4-digit airfoil generation. As for the objective functions, more practical aerodynamic performance should be considered by adding such as the power coefficient of blade in hovering with fixed thrust, rotor stability, and autorotation characteristic. These series of optimization researches can help the design of rotor on general flight of helicopter.

Reference

1. F. H. Schmitz and Y. H. Yu, "Helicopter Impulsive Noise: Theoretical and Experimental Status," NASA TM 84390 and USAAVRADCOR TR 83-A-2, Nov. 1983.
2. J. J. Philippe and A. Vuillet, "Aerodynamic Design of Advanced Rotors with New Tip Shapes," 39th Annual Forum of the American Helicopter Society, St. Louis, Missouri, May 1983.
3. C. Polacsek, J. Zibi, and M. Costes, "Helicopter Rotor Noise Predictions Using 3D Computed Aerodynamic Data for Different Blade Geometries," Proceedings of the 19th European Rotorcraft Forum, Paper No. B3, Como, Italy, September 1993.
4. S. W. Lee, and O.J. Kwon, "Aerodynamic shape optimization of hovering rotor blades in transonic flow using unstructured meshes", AIAA Volume 44 No. 8, Jan. 2006.
5. S. Xue, B. Docker, J. Narramore, "Integrated Aero-Acoustics Rotor Simulation and Design Optimization", 12th AIAA/CEAS Aeroacoustics Conference (27th AIAA Aeroacoustics Conference), 8-10 May, Cambridge, Massachusetts, 2006
6. K. Collins, J. Bain, L. Sankar, T. A. Egolf, R. D. Janakiram, K. Brentner, and L. Lopes, "Pareto Frontier Method for Multi-Disciplinary Optimization of Helicopter Rotors," Presented at the American Helicopter Society Specialist's Conference on Aeromechanics, San Francisco, CA, Jan. 23-25, 2008.
7. C. Yang, T. Aoyama, S. Chae, K. Yee, S. Jeong, and S. Obayashi, "Blade Planform Optimization to Reduce HSI Noise of Helicopter in Hover", the 64th American Helicopter Society Forum, April 29-May 1, 2008, Montreal, Canada
8. T. Aoyama, K. Kawachi, and S. Saito, "Unsteady Calculation for Flow-field of Helicopter Rotor with Various Tip Shapes," Paper No. B03, 18th European Rotorcraft Forum, Avignon, France, September 15-18, 1992.

9. T. W. Purcell, "CFD and Transonic Helicopter Sound," Proceedings of the 14th European Rotorcraft Forum, 1988.
10. H. R. Agarwal, "The Calculation of Transonic Rotor Noise," AIAA Journal, Vol.22, No.7, 1984.
11. F. Farassat, "Generalized functions and Kirchhoff formulas," 2nd AIAA/CEAS Aeroacoustics Conference (17th AIAA Aeroacoustics Conference), AIAA paper 96-1705, 1996.
12. F. Farassat, "Acoustic radiation from rotating blade – The Kirchhoff method in aeroacoustics," Journal of Sound and Vibration, Vol.239, No.4, pp.785-800, 2001.
13. F. Farassat, "Theory of noise generation from moving bodies with an application to helicopter rotors," NASA TR R 451, 1975.
14. S. Jeong, M. Murayama, and K. Yamamoto, "Efficient Optimization Design Method Using Kriging Model," Journal of Aircraft, Vol.42, No.2, pp.413-420, 2005.
15. B. K. Beachkofski, and R. V. Grandhi, "Improved Distributed Hypercube Sampling," 43rd AIAA/ASME/ASCE/AHS/ASC Structures, Structural Dynamics, and Materials Conference, Denver, CO, April 22-25, 2002.
16. D. E. Goldberg, "Genetic Algorithms in Search, Optimization & Machine Learning," Addison-Wesley Publishing, Inc., Reading, 1989.
17. H. Takami, H. Kita, and S. Kobayashi, "Multi-Objective Optimization by Genetic Algorithms: A Review," Proceedings of 1996 IEEE International Conference on Evolutionary Computation, pp. 517-522, 1996.
18. J. Koehler and A. Owen, "Computer Experiments," Handbook of Statistics, 13: Design and Analysis of Experiments, edited by S. Ghosh and C. R. Rao, Elsevier, Amsterdam, pp. 261–308, 1996.
19. Donald, R. J., Matthias S and William J. W, "Efficient Global Optimization of Expensive Black-Box Function," Journal of global optimization, Vol. 13, 1998, pp. 455-492.
20. Matthias, S., William, J. W. and Donald, R. J., "Global Versus Local Search in Constrained Optimization of Computer Models," New Developments and Applications in Experimental Design, edited by N. Flournoy, W.F. Rosenberger, and W.K. Wong , Institute of Mathematical Statistics, Hayward, California, Vol. 34, 1998, pp. 11-25.